

From local to global spatiotemporal chaos in a cardiac tissue model

Zhilin Qu, James N. Weiss, and Alan Garfinkel

Departments of Medicine (Cardiology) and Physiological Science, University of California at Los Angeles, Los Angeles, California 90095

(Received 13 July 1999)

Two kinds of chaos can occur in cardiac tissue, chaotic meander of a single intact spiral wave and chaotic spiral wave breakup. We studied these behaviors in a model of two-dimensional cardiac tissue based on the Luo-Rudy I action potential model. In the chaotic meander regime, chaos is spatially localized to the core of the spiral wave. When persistent spiral wave breakup occurs, there is a transition from local to global spatiotemporal chaos.

PACS number(s): 87.19.Hh, 05.45.Jn, 87.19.Nn

INTRODUCTION

Spiral waves in excitable media are capable of a number of distinct behaviors, some of which are quite complex. Complicated meander patterns with and without spiral wave breakup have been widely observed in computer simulations [1–12], in chemical reactions [13–15], and in cardiac tissue [16–21]. In cardiac tissue, it has been suggested that transitions to chaotic meander and breakup underlie the transition to ventricular fibrillation, the principal cause of sudden cardiac death [4,18,19,22].

The simplest transition in the spiral wave family is from a stable (that is, stationary, periodic) spiral wave to quasiperiodic meander. This has been shown to be a secondary Hopf bifurcation [23,24]. But more complicated spiral wave behaviors, such as hypermeander and breakup, are not well characterized. Most studies that explicitly address the question of chaos in spiral waves have studied the breakup regime [2,11,25]. Recent simulations have shown that self-sustained chaotic meander can occur in a FitzHugh-Nagumo-type (FHN) excitable medium [9]. In cardiac models, complex meandering and spiral wave breakup have been found in a tissue model with Beeler-Reuter (BR) action potential kinetics [5,7,26], with a simplified model [4], and with phase I of the Luo-Rudy (LR1) action potential model [10,12,27,28]. Here we simulated a two-dimensional cardiac tissue model with LR1 kinetics [29]. We found that a transition from quasiperiodic meander to sustained chaotic meander, and then to persistent breakup occurs. In the case of chaotic meander, chaos is localized in the spiral core area. Fully developed spatiotemporal chaos occurs with spiral wave breakup.

MATHEMATICAL MODEL

The partial differential equation for cardiac conduction in homogeneous tissue is [4,5,7,12,26]

$$\partial_t V = -I_{\text{ion}}/C_m + D\nabla^2 V, \quad (1)$$

where V (mV) is membrane potential, $C_m = 1 \mu\text{F cm}^{-2}$ is membrane capacitance, $D = 1 \text{ cm}^2/\text{s}$ is the diffusion constant, and $I_{\text{ion}} (\mu\text{A cm}^{-2})$ is the cellular transmembrane ionic current density. We used the LR1 action potential model [29], in which $I_{\text{ion}} = I_{\text{Na}} + I_{\text{Si}} + I_{\text{K}} + I_{\text{K1}} + I_{\text{Kp}} + I_b$. $I_{\text{Na}} = \bar{G}_{\text{Na}} m^3 h j (V$

$-E_{\text{Na}})$ is the fast inward Na^+ current, $I_{\text{Si}} = \bar{G}_{\text{Si}} df(V - E_{\text{Si}})$ is the slow inward current, which is assumed to be the L -type Ca^{2+} current, $I_{\text{K}} = \bar{G}_{\text{K}} x x_1 (V - E_{\text{K}})$ is the slow outward time-dependent K^+ current, $I_{\text{K1}} = \bar{G}_{\text{K1}} \text{K1}_{\infty} (V - E_{\text{K1}})$ is time-independent K^+ current, $I_{\text{Kp}} = 0.0183 \text{K}_p (V - E_{\text{Kp}})$ is the plateau K^+ current, and $I_b = 0.03921(V + 59.87)$ is the total background current. m , h , j , d , f , and x are the gating variables, satisfying the following type of differential equation:

$$dy/dt = (y_{\infty} - y)/\tau_y, \quad (2)$$

where y represents the gating variables. The ionic concentrations are $[\text{Na}]_i = 18 \text{ mM}$, $[\text{Na}]_o = 140 \text{ mM}$, $[\text{K}]_i = 145 \text{ mM}$, $[\text{K}]_o = 5.4 \text{ mM}$, while the intracellular Ca^{2+} concentration obeys

$$d[\text{Ca}]_i/dt = -10^{-4} I_{\text{Si}} + 0.07(10^{-4} - [\text{Ca}]_i). \quad (3)$$

By setting $[\text{K}]_o = 5.4 \text{ mM}$, the maximum conductance of I_{K} and I_{K1} are $\bar{G}_{\text{K}} = 0.282 \text{ mS/cm}^2$ and $\bar{G}_{\text{K1}} = 0.6047 \text{ mS/cm}^2$. The action potential duration (APD) of the LR1 model is around 360 ms, which is too long to support reentry in relatively small tissue, as has been mentioned by others [10,12,27]. To get an appropriate wavelength, channel conductance parameters must be changed. In this paper, we changed the maximum Na^+ channel conductance to $\bar{G}_{\text{Na}} = 16 \text{ mS/cm}^2$ as in phase II of the Luo and Rudy model [30], and we changed the maximum K^+ channel conductance to $\bar{G}_{\text{K}} = 0.423 \text{ mS/cm}^2$ to shorten the APD. As our control parameter, we used the maximum Ca^{2+} channel conductance \bar{G}_{Si} (in units of mS/cm^2).

NUMERICAL METHODS

We used an operator splitting method to integrate Eq. (1). Equation (1) was split into an ordinary differential equation which is the ionic current term

$$\partial_t V = -I_{\text{ion}}/C_m, \quad (4)$$

and a partial differential equation, which is the diffusion term

$$\partial_t V = D\nabla^2 V. \quad (5)$$

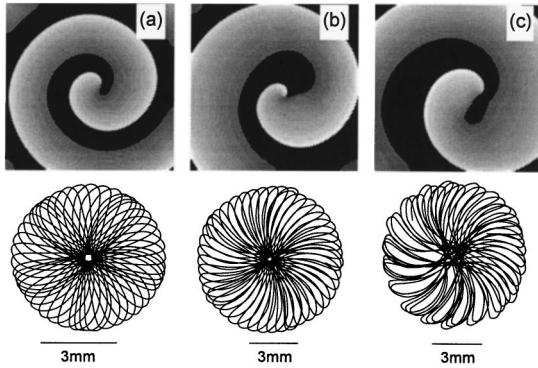


FIG. 1. Spiral wave snapshots (voltage decreases from white to black) and spiral tip trajectories in a 6 cm \times 6 cm tissue for (a) $\bar{G}_{Si}=0.02$, (b) $\bar{G}_{Si}=0.035$, (c) $\bar{G}_{Si}=0.0395$.

The differential equations for the gating variables [Eq. (2)] were integrated with the method of Rush and Larsen [31]. Equations (3) and (4) were integrated with a first order explicit method, using an adaptive time step method. Details of this method were published elsewhere [32]. The time step varied from 0.005 to 0.05 ms. Equation (5) was integrated using the alternating direction implicit method [33] with time step 0.05 ms. The space step was fixed at 0.015 cm. Integration of ODEs and the PDE were carried out alternatively as required by the operator splitting method. No-flux boundary conditions were used.

Spiral waves were initiated by the cross field protocol [17]. Tip trajectories were measured using the intersection of two isovoltage contour lines 2 ms apart. The threshold for the isovoltage contour lines is -30 mV. Cycle length (CL) was defined as the time interval between the upstrokes of two successive action potentials. A threshold of -72 mV was used to define CL. We found that all choices of isovoltage countour threshold between -20 and -40 mV gave qualitatively similar results, as did choices of CL threshold between -50 and -75 mV (results not shown).

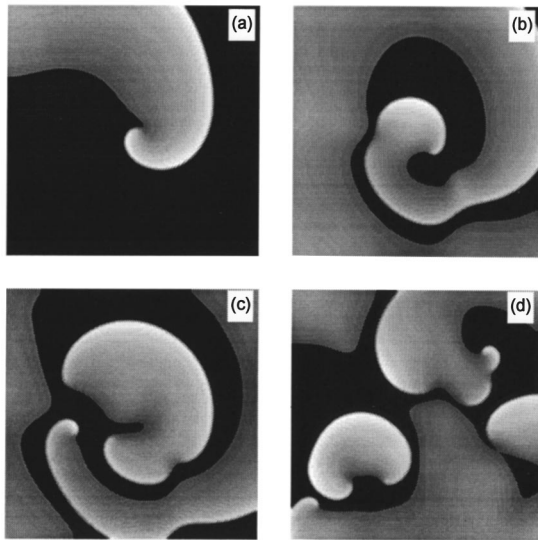


FIG. 2. A single spiral wave breaks into multiple spiral waves in a 6 \times 6 cm tissue for $\bar{G}_{Si}=0.052$. (a) $t=100$ ms, (b) $t=210$ ms, (c) $t=240$ ms, and (d) $t=1000$ ms. We set $t=0$ when the second pulse initiating the spiral wave is given.

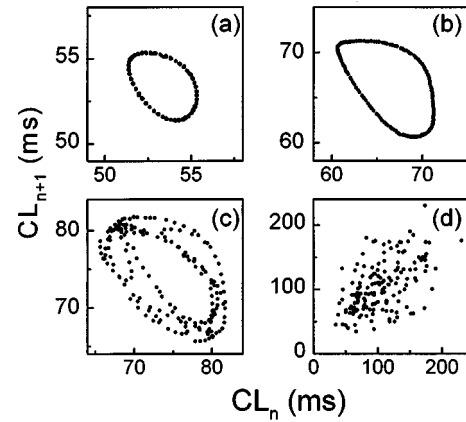


FIG. 3. CL return maps for $\bar{G}_{Si}=0.02$ (a), 0.035 (b), 0.0395 (c), and 0.052 (d). In these figures, the first 30 transient CLs were dropped.

RESULTS

As \bar{G}_{Si} increases, the trajectory of the spiral tip becomes more and more complex, becoming irregular at $\bar{G}_{Si}=0.0395$ (Fig. 1). (A similar result has been found in a BR-based system [5].) As \bar{G}_{Si} increases further, a single intact spiral wave cannot exist in this tissue, and spontaneous spiral wave breakup occurs (Fig. 2). This spiral wave breakup creates a regime of multiple spiral waves, in which spirals are continually being created and destroyed. In this regime, the spiral waves rotate very irregularly and their number is also irregular (see Fig. 7 below). To show how complex behavior develops, we studied CL return maps for increasing values of \bar{G}_{Si} (Fig. 3). For $\bar{G}_{Si}=0.02$ and 0.035, the return maps were simple closed ringlike structures, indicating quasiperiodic behavior. But when \bar{G}_{Si} was increased to 0.0395, the ring structure became partly, but only partly, obscured by irregular behavior. When spiral wave breakup occurred, the CL return map shows a completely irregular pattern.

To determine when chaos occurs in the transition from quasiperiodic meander to irregular meander, we calculated the maximum Lyapunov exponent λ . It is extremely difficult to use Eqs. (1)–(3) to compute λ in the tangent space, as defined in text books [34], i.e.,

$$\lambda = \lim_{t \rightarrow \infty} \frac{1}{t} \ln \frac{\|\mathbf{w}(t)\|}{\|\mathbf{w}(0)\|},$$

where $\mathbf{w}(0)$ is the initial perturbation vector and $\mathbf{w}(t)$ is the final perturbation vector. We used an alternative method to

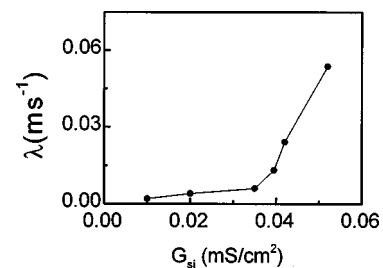


FIG. 4. λ versus \bar{G}_{Si} .

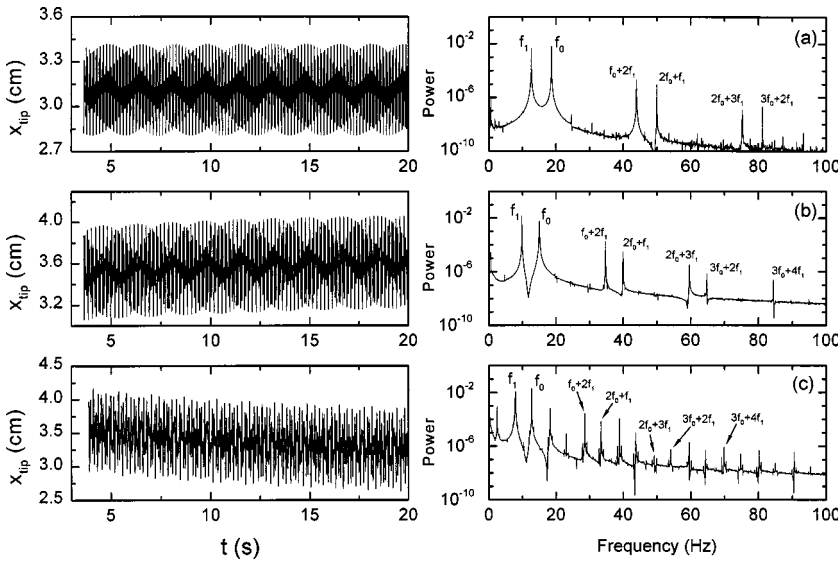


FIG. 5. x coordinate of the spiral tips (left) and their FFT power spectrum over 20 sec (right). Tissue size 6 cm \times 6 cm. (a) $\bar{G}_{Si}=0.02$; (b) $\bar{G}_{Si}=0.035$; (c) $\bar{G}_{Si}=0.0395$.

calculate λ [35]. Figure 4 shows λ versus \bar{G}_{Si} . In the quasiperiodic regime, the calculated value of λ is zero, within numerical error. When the irregular meander begins, λ increases quickly as \bar{G}_{Si} increases, showing that the chaotic motion becomes more violent with increasing \bar{G}_{Si} .

In order to study the transition from quasiperiodicity to chaos, we first verified that the pretransition behavior is truly quasiperiodic. For the lower values of \bar{G}_{Si} , all the peaks in the Fourier spectrum can be expressed as $mf_0 + nf_1$, with m and n integers [34], showing that the motion is quasiperiodic with the basic frequency f_0 and modulating frequency f_1 . But for $\bar{G}_{Si}=0.0395$, not all the peaks can be expressed as $mf_0 + nf_1$ [Fig. 5(c)], and so new frequencies have emerged.

The irregular motion of the tip persists for the entire 20 simulated seconds of activity (about 250 rotations). While we suspect that this is not likely to be a transient, we cannot rule out the existence of ‘‘chaotic supertransients’’ as have been seen in other spatiotemporal examples [36,37]. Note that the tip coordinate displays a small long-term drift, as has been observed in the FHN-type model [9]. This drift may be due to the interactions of the spiral wave with the no-flux boundary.

To further investigate chaos in this system, we used perturbations to study the system response. Figure 6 shows the effects of perturbations to a quasiperiodically meandering spiral wave and to a chaotically meandering spiral wave. A perturbation to a quasiperiodically meandering spiral wave did not give rise to a clearly observable discrepancy from the original time series of action potentials. Instead, there is a small phase shift in the tip trajectory [Fig. 6(a)]. But a perturbation to a chaotically meandering spiral wave close to the spiral tip gave rise to larger differences, in both the time series of action potentials and in tip trajectories [Fig. 6(b)]. This again shows that irregular meander is chaotic. However, if a perturbation was delivered in a place far from the tip, there was no effect on either the time series of action potentials or on the tip trajectories [Fig. 6(c)]. This indicates that chaos in a chaotically meandering spiral wave is localized in the core area, not in the arm far from the core.

In contrast to the chaotic meander case, in the breakup regime, a local perturbation in the tissue propagates quickly

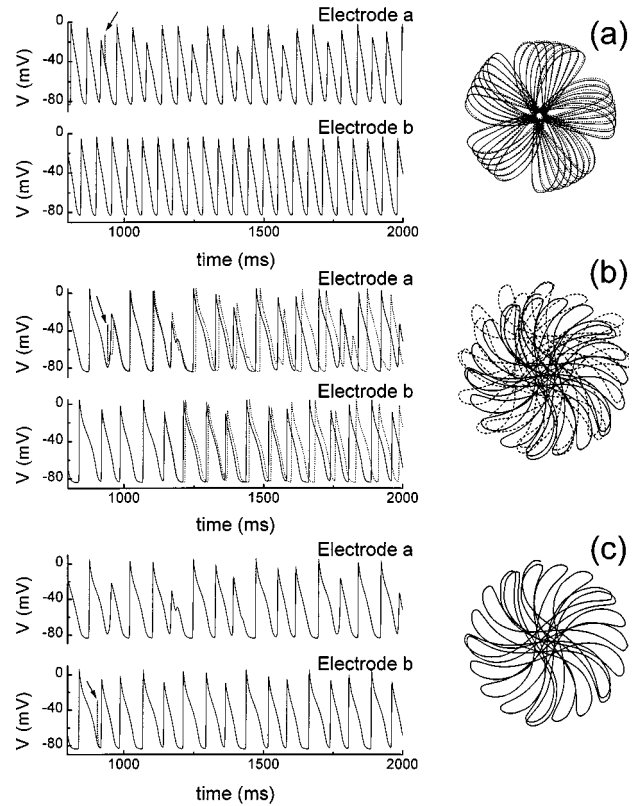


FIG. 6. A local perturbation was given in either electrode a or b to demonstrate the ‘‘butterfly effect’’ (sensitive dependence on initial conditions, often held to be defining of chaos). Voltage traces (left) and tip trajectories (right) are shown. The tissue size is 6 cm \times 6 cm. Perturbation was given in one computational ‘‘cell’’ (0.015 cm \times 0.015 cm), by holding the voltage at 0 mV for 2 ms in that site. Electrode a is at $x=3.6$ cm and $y=3$ cm which is very close to the spiral tip area; electrode b is at $x=y=0.75$ cm which is far away from the spiral tip area. Solid lines are before perturbation, the dashed lines are after perturbation. Arrows indicate the time at which the perturbation was given. (a) $\bar{G}_{Si}=0.02$, perturbation was given at electrode a; (b) $\bar{G}_{Si}=0.04$, perturbation was given at electrode a; (c) the same as (b) but the perturbation was given at electrode b.

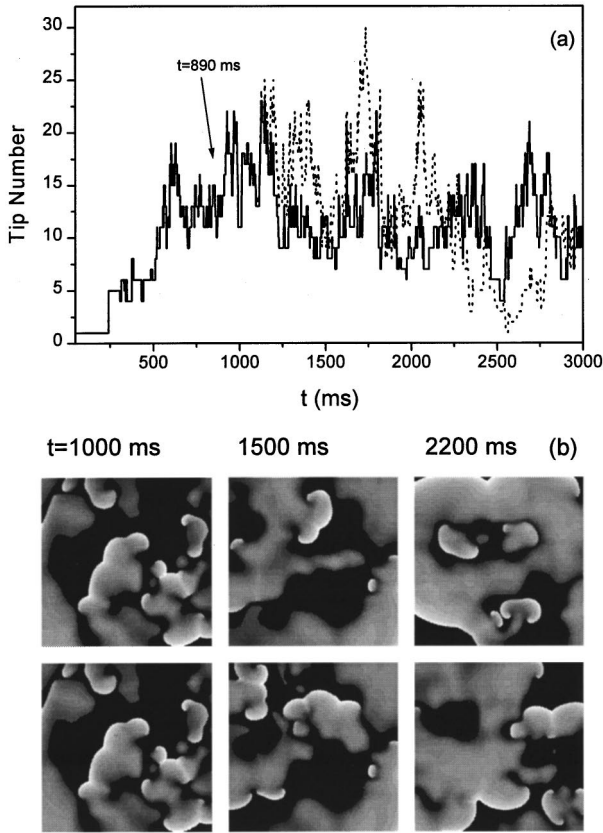


FIG. 7. (a) Tip numbers versus time for the cases with (solid line) and without (dotted line) added local perturbation. (b) Snapshots for $t=1000$, 1500 , 2200 ms. Upper panel is the case with no perturbation, lower panel is the case with perturbation. The local perturbation was delivered at 890 ms in area of $0.06\text{ cm}\times 0.06\text{ cm}$ in the center of the tissue. We hold the voltage at that area at 0 mV for 2 ms , which did not create any new waves and did not significantly change the snapshot, as shown in the results above.

in both time and space, leading to very divergent spatiotemporal patterns. Figure 7 shows the tip number versus time for the cases with and without perturbation, and some voltage snapshots. Although the perturbation was delivered at 0.89 s , the spatial patterns are almost identical at 1 s . At 1.5 s , part of the pattern differs, and at 2.2 s , the spatial patterns are completely different.

We also initiated multiple spiral waves in the tissue to study their interactions. We first initiated two counter-rotating spiral waves which were symmetric with respect to the central horizontal line, i.e., one is the other's mirror image. With this symmetry, $\Delta x = x_1 - x_2$ must be zero and $\langle y \rangle = (y_1 + y_2)/2$ must be a constant, where (x_1, y_1) and (x_2, y_2) are the tip positions of the two spiral waves. When we initiated such a pair of spirals in the chaotic meander regime, neither $\Delta x = 0$ nor $\langle y \rangle = \text{const}$ were maintained; instead, these quantities oscillated violently in a chaotic manner indicating that the pair of synchronously rotating spiral waves was desynchronized (Fig. 8). This happened because numerical error in the simulation was amplified by the chaotic behavior of the spiral waves. A careful examination of our data for both Δx and $\langle y \rangle$ shows that Δx is exactly zero and $\langle y \rangle$ is exactly 3.0 within the first 100 ms (see the inset in Fig. 8). Afterwards errors occurred in either Δx or $\langle y \rangle$,

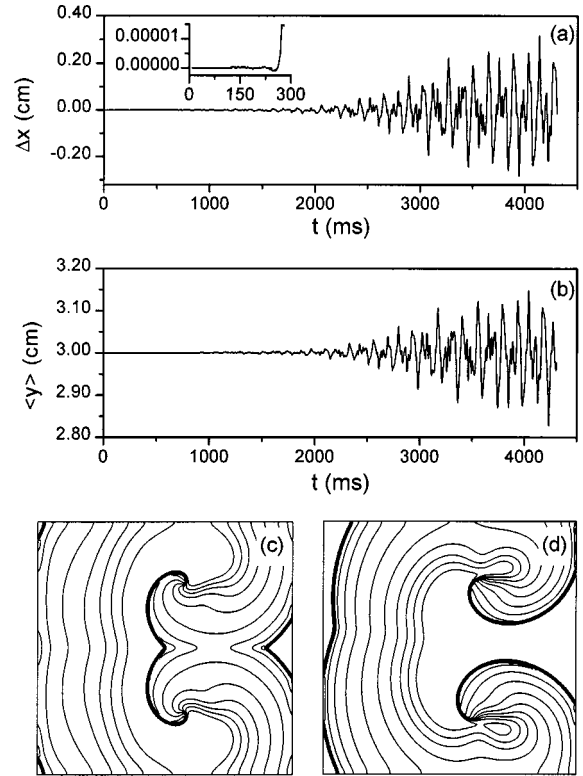


FIG. 8. (a) and (b) Δx and $\langle y \rangle$ versus time. The inset in (a) is an enlarged view of Δx for the first 300 ms . (c) Contour plots of spiral waves for $t=700$ and 4000 ms . At $t=700\text{ ms}$, the spiral waves are symmetric with respect to the center line of tissue in x direction, at $t=4000\text{ ms}$, this symmetry was lost. Tissue size is $6\text{ cm}\times 6\text{ cm}$ and $\bar{C}_{si}=0.04$.

which became amplified by the chaotic nature of the spiral wave. We carried out the same simulation in the quasiperiodic meander regime, and Δx always remained on the order of 10^{-4} cm , which is the numerical error. To study how one spiral wave responded to the other in the chaotic meander regime, we gave a perturbation to *one* of the two spiral waves shown in Fig. 8. Although the perturbation made the two spiral waves desynchronize [Figs. 9(a) and 9(b)], the unperturbed spiral wave was largely unaffected [Fig. 9(d)]. In Figs. 9(c) and 9(d), we plotted the two spiral tip trajectories from $t=2000$ to 4000 ms for the cases with and without perturbation. The tip trajectory of the perturbed spiral wave diverges strongly from the original trajectory, but the tip trajectory of the unperturbed spiral wave is almost identical to the original tip trajectory.

We also initiated four spiral waves in the tissue to study their interactions. A perturbation was delivered to the core area of one of the four spiral waves at 200 ms after the initiation. This perturbation is strong enough to break the initial symmetry but not to create new spiral waves. In the quasiperiodic meander regime, this perturbation only broke the initial symmetry, and made the waves rotate in different phases [Figs. 10(a) and 10(b)]. But in the chaotic meander regime, the situation is different. A suitable perturbation may cause spiral wave breakup. In Figs. 10(c) and 10(d), we show one such simulation. 600 ms after the perturbation, spontaneous spiral wave breakup occurred [Fig. 10(c)] and the number of tips changed quickly with time [Fig. 10(d)], simi-

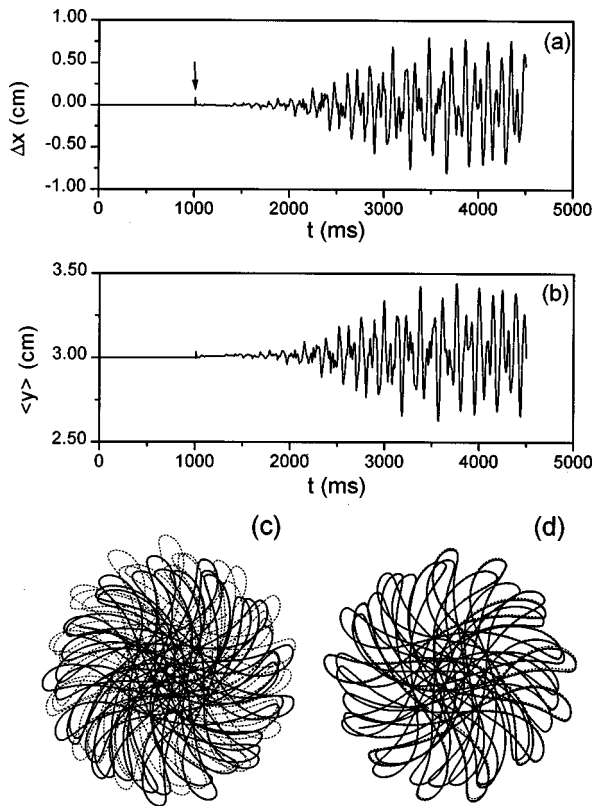


FIG. 9. (a) and (b) Δx and $\langle y \rangle$ versus time, for the pair of spiral waves shown in Fig. 8, one of which is perturbed. (c) and (d) show tip trajectories for the simulation without perturbation (solid line) and with perturbation (dashed line). The perturbation was delivered at an area of $0.06 \text{ cm} \times 0.06 \text{ cm}$ close to one of the tips of the two spiral waves shown in Fig. 8, by holding the voltage at 0 mV for 2 ms . Tip trajectories shown in (c) and (d) are from $t=2000$ to 4000 ms . The arrow in (a) shows the time at which the perturbation was given. The parameters are the same as in Fig. 8.

lar to what occurred in the breakup regime (Fig. 7). However, breakup in the chaotic meander regime was not inevitable; it required two spiral waves to be close enough to invade each other's territory and interact strongly. If the chaotically meandering spiral waves are far apart, they rotate independently. Chaotic meander is crucial for this type of breakup, because it amplifies the perturbation and makes the spiral wave move in a very different phase. Such perturbation-induced breakup was never observed in the quasiperiodic meander regime in our simulations.

CONCLUSION

We have shown, in a cardiac tissue model with LR1 kinetics, that a transition from quasiperiodic meander to cha-

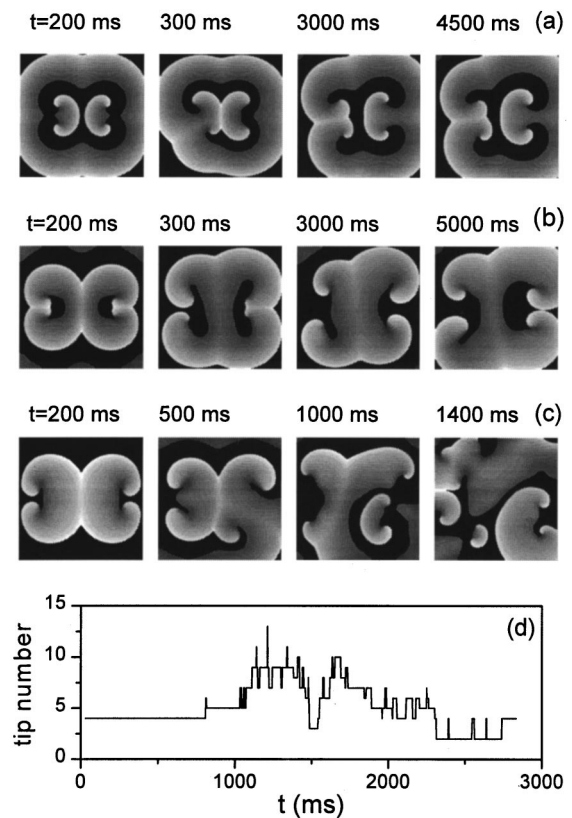


FIG. 10. Snap shots of spiral waves at different time for $\bar{G}_{Si} = 0.02$ (a), $\bar{G}_{Si} = 0.035$ (b), and $\bar{G}_{Si} = 0.04$ (c). (d) Number of spiral tips versus time for $\bar{G}_{Si} = 0.04$. Tissue size is $6 \text{ cm} \times 6 \text{ cm}$. Perturbations were given to one of the four spiral waves at 200 ms .

otic meander occurs as \bar{G}_{Si} is increased. This chaotic meander is "local chaos," in the sense that the chaos is localized to the spiral core. Spectral analysis applied to the transition shows that a two-frequency quasiperiodic motion undergoes a transition to weakly chaotic motion. The weakly chaotic state displays at least one new frequency, which would suggest a "quasiperiodic transition to chaos" [38]. Several distinct pathways from quasiperiodicity to chaos, such as "torus doubling" and "torus breakdown" have been identified [39]. A "torus breakdown" transition from quasiperiodicity to chaos was previously found in a cardiac tissue model based on simplified three-variable cell kinetics [19], but none of these well-known scenarios seems to be present here in the model with LR1 kinetics.

ACKNOWLEDGMENTS

This research was supported by NIH SCOR in Sudden Cardiac Death P50 HL52319 and by the American Heart Association, Western States Affiliate to Z.Q.

[1] A. T. Winfree, *Chaos* **1**, 303 (1991).
 [2] A. V. Panfilov and A. V. Holden, *Int. J. Bifurcation Chaos Appl. Sci. Eng.* **1**, 219 (1991).
 [3] H. Ito and L. Glass, *Phys. Rev. Lett.* **66**, 671 (1991).
 [4] A. Karma, *Chaos* **4**, 461 (1994).
 [5] I. R. Efimov, V. I. Krinsky, and J. Jalife, *Chaos Solitons Fractals* **5**, 513 (1995).

[6] H. Zhang and A. V. Holden, *Chaos Solitons Fractals* **5**, 661 (1995).
 [7] M. Courtemanche, *Chaos* **6**, 579 (1996).
 [8] A. F. M. Maree and A. V. Panfilov, *Phys. Rev. Lett.* **78**, 1819 (1997).
 [9] V. N. Biktashev and A. V. Holden, *Physica D* **116**, 342 (1998).
 [10] J. Beaumont *et al.*, *Biophys. J.* **75**, 1 (1998).

- [11] M. C. Strain and H. S. Greenside, *Phys. Rev. Lett.* **80**, 2306 (1998).
- [12] Z. Qu, J. N. Weiss, and A. Garfinkel, *Am. J. Physiol.* **276**, H269 (1999).
- [13] K. I. Agladze, V. I. Krinsky, and A. M. Pertsov, *Nature (London)* **308**, 834 (1984).
- [14] M. Markus, G. Kloss, and I. Kusch, *Nature (London)* **371**, 402 (1994).
- [15] G. Li *et al.*, *Phys. Rev. Lett.* **77**, 2105 (1996).
- [16] J. M. Davidenko *et al.*, *Nature (London)* **355**, 349 (1992).
- [17] A. M. Pertsov *et al.*, *Circ. Res.* **72**, 631 (1993).
- [18] R. A. Gray and J. Jalife, *Int. J. Bifurcation Chaos Appl. Sci. Eng.* **6**, 415 (1996).
- [19] A. Garfinkel *et al.*, *J. Clin. Invest.* **99**, 305 (1997).
- [20] Y. H. Kim *et al.*, *J. Clin. Invest.* **100**, 2486 (1997).
- [21] P.-S. Chen *et al.*, *Chaos* **8**, 127 (1998).
- [22] J. E. Poole and G. H. Bardy, in *Cardiac Electrophysiology: From Cell to Bedside*, edited by D. P. Zipes and J. Jalife (Saunders, Philadelphia, 1995), Vol. 2, p. 812.
- [23] D. Barkley, *Phys. Rev. Lett.* **68**, 2090 (1992).
- [24] A. Karma, *Phys. Rev. Lett.* **65**, 2824 (1990).
- [25] M. Bar and M. Eiswirth, *Phys. Rev. E* **48**, R1635 (1993).
- [26] M. Courtemanche and A. T. Winfree, *Int. J. Bifurcation Chaos Appl. Sci. Eng.* **1**, 431 (1991).
- [27] A. Xu and M. R. Guevara, *Chaos* **8**, 157 (1998).
- [28] F. Xie, Z. Qu, and A. Garfinkel, *Phys. Rev. E* **58**, 6355 (1998).
- [29] C. H. Luo and Y. Rudy, *Circ. Res.* **68**, 1501 (1991).
- [30] C. H. Luo and Y. Rudy, *Circ. Res.* **74**, 1071 (1994).
- [31] S. Rush and H. Larsen, *IEEE Trans. Biomed. Eng.* **25**, 389 (1978).
- [32] Z. Qu and A. Garfinkel, *IEEE Trans. Biomed. Eng.* **46**, 1166 (1999).
- [33] J. W. Thomas, *Numerical Partial Differential Equations* (Springer-Verlag, New York, 1995).
- [34] P. Berge, Y. Pomeau, and C. Vidal, *Order within Chaos: Towards a Deterministic Approach to Turbulence* (Wiley, New York, 1984).
- [35] We calculated λ by simultaneously integrating two copies of Eqs. (1)–(3) with the same initial condition, and gave a small perturbation to one of the integrations. We used the same definition of the maximum Lyapunov exponent as
- $$\lambda = \lim_{t \rightarrow \infty} \frac{1}{t} \ln \frac{\|w(t)\|}{\|w(0)\|} \approx \sum_{n \rightarrow \infty} \frac{\lambda_n}{n},$$
- where
- $$\lambda_n = \frac{1}{\Delta T} \ln \frac{\|w(n\Delta T)\|}{\|w((n-1)\Delta T)\|}.$$
- Here $w[(n-1)\Delta T]$ is the perturbation given at $(n-1)\Delta T$ and $w(n\Delta T)$ is the difference of the integration at $n\Delta T$. At $n\Delta T$, we rescale $w(n\Delta T)$ to be very small and reset the simulation. We used $\Delta T = 20$ ms.
- [36] J. P. Crutchfield and K. Kaneko, *Phys. Rev. Lett.* **60**, 2715 (1988).
- [37] Z. Qu and G. Hu, *Phys. Rev. E* **49**, 1099 (1994).
- [38] D. Ruelle and F. Takens, *Commun. Math. Phys.* **20**, 167 (1971).
- [39] R. C. Hilborn, *Chaos and Nonlinear Dynamics* (Oxford University Press, New York, 1994).